Applied Surface Science 257 (2011) 7343–7349

Contents lists available at ScienceDirect

Applied Surface Science

journal homepage: www.elsevier.com/locate/apsusc

Optical and structural properties of Si-doped ZnO thin films

I. Sorar [a,b,*], D. Saygin-Hinczewski [b], M. Hinczewski [c,d], F.Z. Tepehan [b]

[a] Department of Physics, Mustafa Kemal University, Antakya 31034, Hatay, Turkey
[b] Department of Physics, Istanbul Technical University, Maslak 34469, Istanbul, Turkey
[c] Feza Gürsey Research Institute, TÜBİTAK–Bosphorus University, Çengelköy 34680, Istanbul, Turkey
[d] Institute for Physical Science and Technology, University of Maryland, College Park, MD 20742, USA

ARTICLE INFO

Article history:
Received 11 December 2010
Received in revised form 28 February 2011
Accepted 29 March 2011
Available online 4 April 2011

Keywords:
Zinc oxide
Sol–gel
Si-doped ZnO
Optical properties
Structural properties
Tauc–Lorentz dielectric model

ABSTRACT

▸ Thin films of Si-doped ZnO were prepared by the sol–gel spin coating method. ▸ The optical and structural properties of the films were investigated to see the effects of Si dopant concentration for three different heat treatments: 250, 350, and 550 °C. ▸ The optical characteristics for all the films were modeled using a Tauc–Lorentz-based dielectric function and an exponential Urbach tail in the sub-gap regime.

Abstract: Transparent thin films of Si-doped ZnO were prepared by the sol–gel spin coating method. The optical and structural properties of the films were investigated to see the effects of Si dopant concentration for three different heat treatments: 250, 350, and 550 °C. Doping is most significant at the highest annealing temperature, where the structure of the films is crystalline at low Si values, and deteriorates as Si levels are increased. Optically, the result is increased transmittance and decreased reflectance with doping for the near-UV and visible ranges. The large changes in the near-UV region (20–50% increase in transmittance relative to pure ZnO) are due to weaker excitonic absorption as crystallinity is destroyed by doping. The films at 250 and 350 ° C were amorphous, but the 350 ° C samples showed optical trends qualitatively similar to 550 ° C (though less pronounced). Band gaps were shifted slightly upwards with doping, though at higher annealing temperatures the values remained within 2% of the 3.3 eV pure ZnO result at all Si levels. AFM measurements of RMS surface roughness varied in a small range from $\lesssim 1$ to 7 nm, with the roughest samples being pure ZnO at 250 °C, and low Si dopings at 550 °C. The optical characteristics for all the films, regardless of heat treatment or doping, were successfully modeled using a Tauc–Lorentz-based dielectric function, consisting of two oscillator terms describing near-band-gap absorption, and an exponential Urbach tail in the sub-gap regime.

© 2011 Elsevier B.V. All rights reserved.

1. Introduction

Due to its optical and electrical properties, zinc oxide (ZnO) is an important technological material. It has been widely used in devices like liquid-crystal display (LCD) panels [1], photovoltaic cells [2], and optical filters [3]. In order to optimize ZnO characteristics for specific applications, a variety of different dopants and preparation techniques have been explored. For the case of Si doping, ZnO films produced through RF magnetron sputtering exhibit high conductivity and transparency [4,5], while those grown by sequential pulsed laser deposition have been proposed as candidates for transparent conducting electrodes (TCEs) [6]. As a co-dopant with Al, Si enhanced the spatial distribution and stability of resistivity in RF magnetron sputtered ZnO films, relevant to practical implementation in LCDs [7]. Earlier research also focused on the synthesis of Si-doped ZnO nanocomposites [8–10] and nanorods [11].

In the present work we examine Si-doped ZnO thin films produced through sol–gel spin coating, a method notable for its efficiency, low cost, compositional control, and easy extension to multilayer structures [12]. While the optical properties of pure sol–gel derived ZnO films have been widely studied [13–15], less is known about the Si-doped case. Our work helps fill this gap by reporting the structural and optical properties of sol–gel Si-doped ZnO films, and their dependence on the heat treatment protocol. We used Si doping values of 0.8%, 1.6%, 3.2% and 6.4%, and three different annealing temperatures: 250, 350 and 550 °C. To accurately extract optical properties, we adapted the double Tauc–Lorentz–Urbach oscillator (DTLU) dielectric model, first applied in the context of pure and doped WO_3 films [16]. This is an extension of the single oscillator TLU model [17], which has proven effective in analyzing pure ZnO films [3].

* Corresponding author at: Department of Physics, Mustafa Kemal University, Antakya 31034, Hatay, Turkey.
E-mail addresses: sorar@itu.edu.tr, idrissorar@gmail.com (I. Sorar).

0169-4332/$ – see front matter © 2011 Elsevier B.V. All rights reserved.
doi:10.1016/j.apsusc.2011.03.142

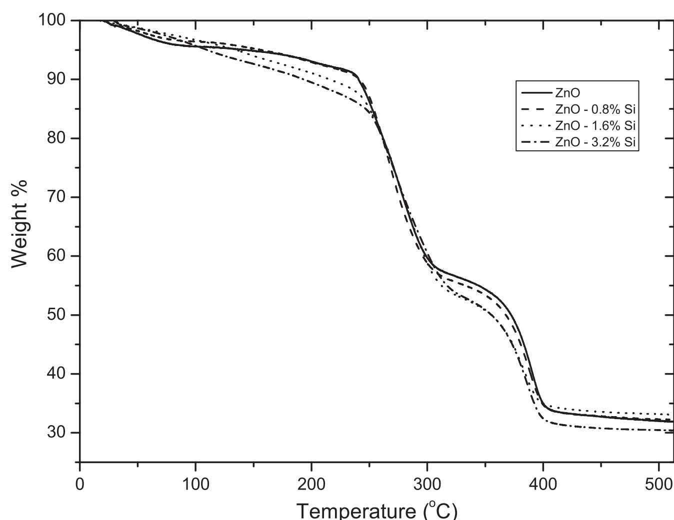

Fig. 1. Thermogravimetric analysis (TGA) graph of the pure and Si-doped ZnO gel.

Table 1
Best-fit parameters of the DTLU model for ZnO:Si thin films annealed at various temperatures *T*. All parameters are in units of eV, except for d_{rough}, which is in units of nm. The latter parameter only appears in cases where corrections due to a surface roughness overlayer could be extrapolated from the experimental data. Of the 12 parameters in the DTLU model, 11 are shown here. The remaining one is the layer thickness *d*, which is listed in Table 2.

T (°C)	Si %	A_1	E_{01}	E_{g1}	Γ_1	A_2	E_{02}	E_{g2}	Γ_2	E_t	E_u	d_{rough}
250	0.0	0.72	3.17	2.86	0.97	107	8.09	4.29	13.87	4.70	0.65	–
	0.8	0.66	3.48	2.47	1.55	102	6.82	4.11	8.03	4.68	0.23	–
	1.6	0.49	3.50	2.51	1.02	102	6.88	4.15	7.48	4.45	0.47	–
	3.2	0.68	3.52	2.51	1.04	103	6.99	4.12	8.38	4.68	0.31	–
	6.4	0.66	3.52	2.92	0.56	103	6.95	4.11	8.36	4.74	0.50	–
350	0.0	38	3.35	3.16	0.38	105	5.76	3.70	11.02	4.40	0.43	–
	0.8	26	3.38	3.14	0.45	97	5.36	3.68	9.46	4.28	0.35	–
	1.6	23	3.39	3.14	0.47	97	5.33	3.67	9.56	4.28	0.35	–
	3.2	22	3.40	3.15	0.49	97	5.35	3.68	9.54	4.29	0.38	–
	6.4	21	3.41	3.17	0.51	99	5.48	3.70	9.67	4.25	0.38	–
550	0.0	44	3.34	3.12	0.32	90	4.85	3.50	8.78	4.22	0.34	–
	0.8	26	3.36	3.09	0.45	87	5.38	3.77	10.77	4.41	0.43	13
	1.6	23	3.36	3.11	0.45	92	5.39	3.77	10.78	4.38	0.53	30
	3.2	19	3.35	3.17	0.44	103	5.74	3.77	11.47	4.26	0.50	35
	6.4	19	3.37	3.18	0.46	95	5.21	3.75	6.51	4.13	0.33	43

2. Experimental procedure

Zinc acetate dihydrate (ZnAc, $Zn(CH_3COO)_2{\cdot}2H_2O$, 98%, Sigma-Aldrich) and tetraethyl orthosilicate (TEOS, $Si(OC_2H_5)_4$, 99.999%, Aldrich) were used as starting materials. Each solution was prepared by dissolving 4 mmol of zinc acetate dihydrate in 10 mL of 2-propanol (99.5%, Aldrich) and stirring by a magnetic stirrer at 60 °C for 10 min. During stirring, 4 mmol of diethanolamine (DEA, 99%, Aldrich) was added drop by drop to the solution. The 1:1 mole ratio of ZnAc:DEA was chosen since the resulting films have good aging characteristics [18]. Afterwards, TEOS were added to give one of four different mole ratios of TEOS to ZnAc: 0.8%, 1.6%, 3.2%, and 6.4%. The solution was stirred an additional 10 min, during which time distilled water was slowly added to it. Finally, a clear and homogeneous liquid was obtained. The solution was left on the magnetic stirrer to cool down slowly.

The solution compositions were checked through inductively coupled plasma optical emission spectroscopy (ICP-OES) using a Vista-MPX (Varian, US) system. For the 0.8%, 1.6%, 3.2%, and 6.4% TEOS:ZnAc doping values, the measured Si:Zn concentration ratios in solution were 0.31%, 0.58%, 1.22% and 2.63%, which agree well with the expected values of 0.345%, 0.690%, 1.38% and 2.76%.

The thin films were deposited through the sol–gel spin coating method. The solution was dropped onto Corning 2947 glass sub-

Table 2
Thickness *d*, refractive index $n(\lambda = 550\,nm)$, absorption coefficient $\alpha(\lambda = 350\,nm)$, band gap E_g, and surface RMS roughness values of ZnO:Si thin films annealed at various temperatures *T*.

T (°C)	Si %	d (nm)	n	α (nm^{-1})	E_g (eV)	RMS (nm)
250	0.0	292	1.57	0.35×10^{-3}	3.15 ± 0.07	7.3
	0.8	245	1.60	0.43×10^{-3}	3.19 ± 0.07	0.2
	1.6	223	1.61	0.54×10^{-3}	3.22 ± 0.03	0.3
	3.2	216	1.62	0.63×10^{-3}	3.24 ± 0.04	0.4
	6.4	196	1.62	0.68×10^{-3}	3.32 ± 0.04	0.4
350	0.0	108	1.61	6.38×10^{-3}	3.31 ± 0.01	0.5
	0.8	116	1.56	5.48×10^{-3}	3.33 ± 0.01	0.9
	1.6	114	1.55	5.10×10^{-3}	3.33 ± 0.01	0.7
	3.2	112	1.55	4.60×10^{-3}	3.34 ± 0.01	0.4
	6.4	115	1.56	3.96×10^{-3}	3.36 ± 0.01	0.4
550	0.0	87	1.55	8.68×10^{-3}	3.29 ± 0.01	4.7
	0.8	101	1.49	6.63×10^{-3}	3.30 ± 0.01	4.5
	1.6	95	1.50	5.49×10^{-3}	3.30 ± 0.01	4.5
	3.2	130	1.55	3.31×10^{-3}	3.31 ± 0.01	1.2
	6.4	126	1.54	3.24×10^{-3}	3.34 ± 0.01	1.2

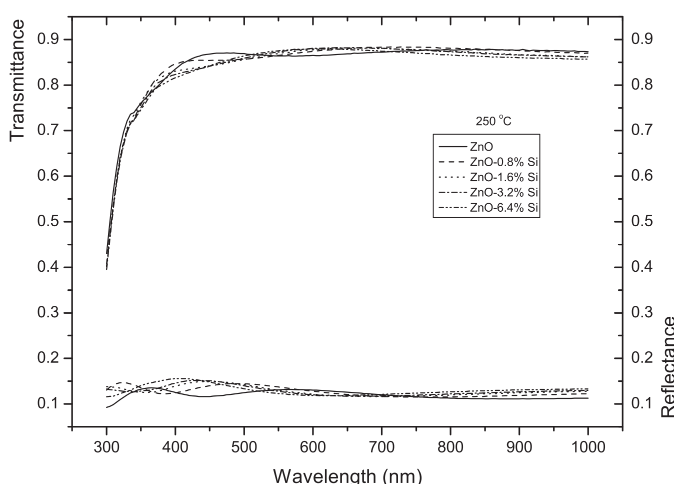

Fig. 2. Transmittance and reflectance spectra of ZnO:Si thin films annealed at 250 °C.

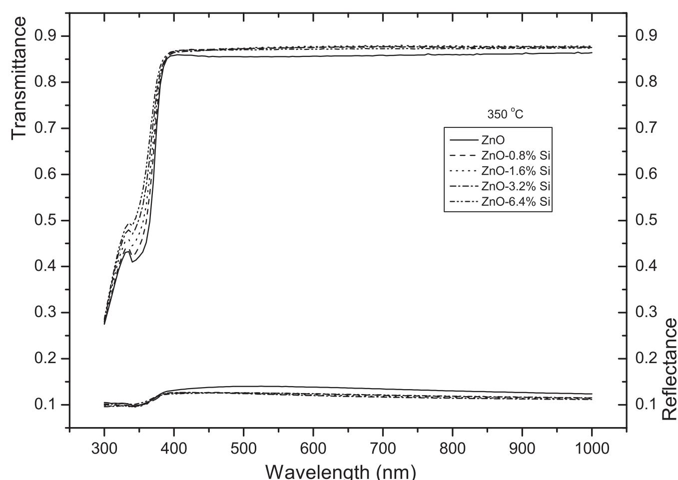

Fig. 3. Transmittance and reflectance spectra of ZnO:Si thin films annealed at 350 °C.

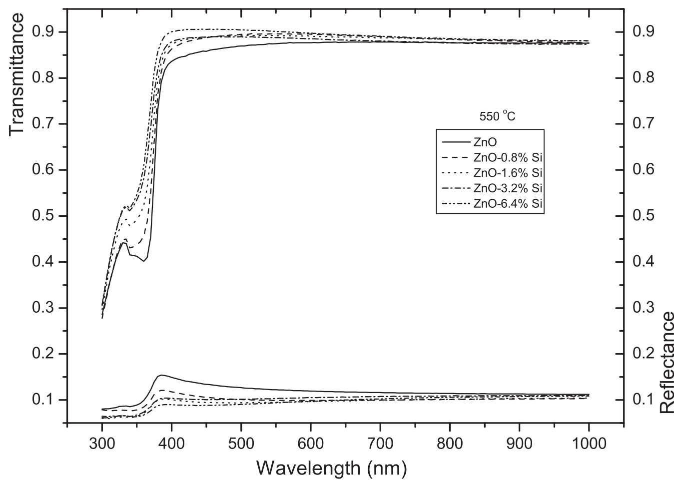

Fig. 4. Transmittance and reflectance spectra of ZnO:Si thin films annealed at 550 °C.

strates on the spin coater, rotating at 2000 rpm for 10 s. The films were dried at 250 ° C for 1 min to evaporate the solvent and remove organic residuals. The coating and drying process was repeated five times. Finally, the films were heat treated at 250, 350, or 500 ° C for 1 h. These temperatures were chosen to correspond to features revealed by thermogravimetric analysis (TGA) of the ZnO:Si gels, given in Fig. 1. Just above 250 ° C there is rapid weight loss due to the evaporation of residual solvent and DEA; the similarly rapid loss above 350 ° C is due to evaporation of residual organic compounds. The third temperature value of 550 ° C is chosen to be clearly in the crystallized regime, where the weight has stabilized. There are no significant differences between the TGA of the ZnO and ZnO:Si

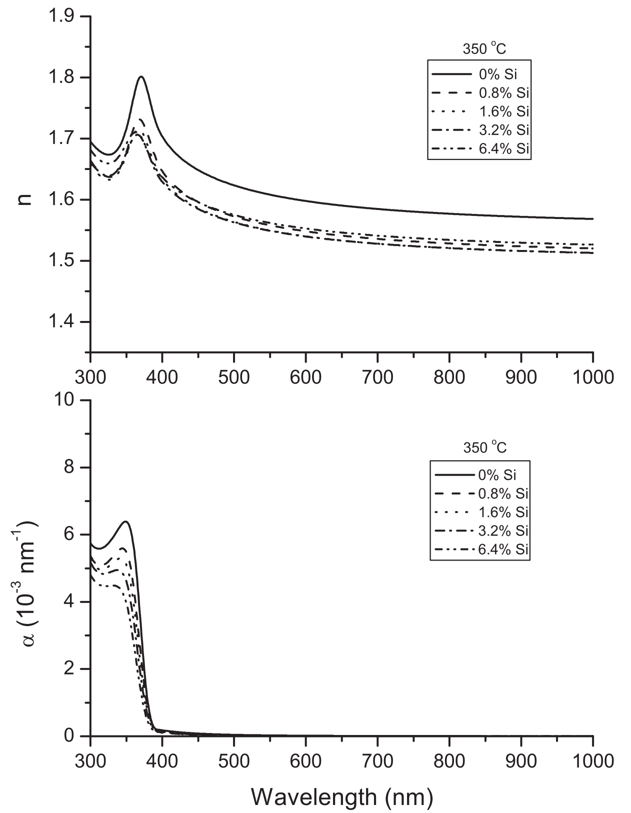

Fig. 6. Refractive index n and absorption coefficient α of ZnO:Si thin films annealed at 350 °C.

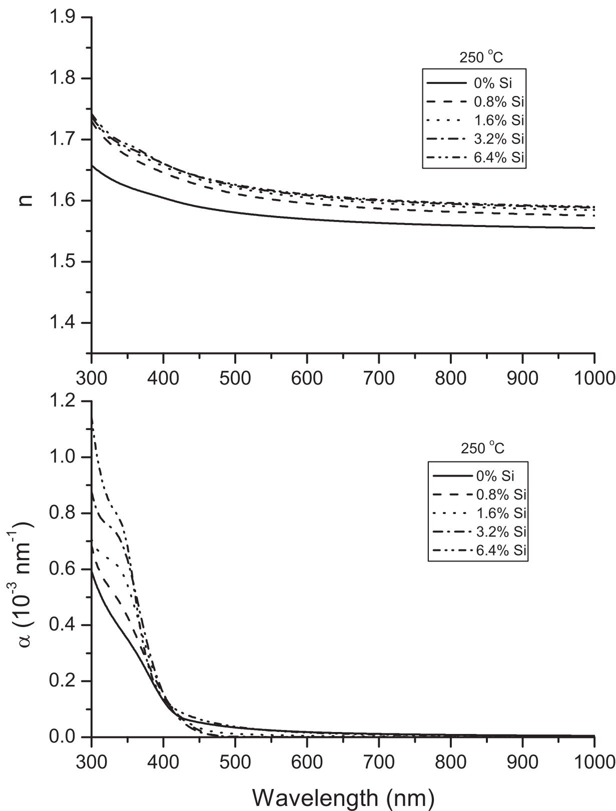

Fig. 5. Refractive index n and absorption coefficient α of ZnO:Si thin films annealed at 250 °C.

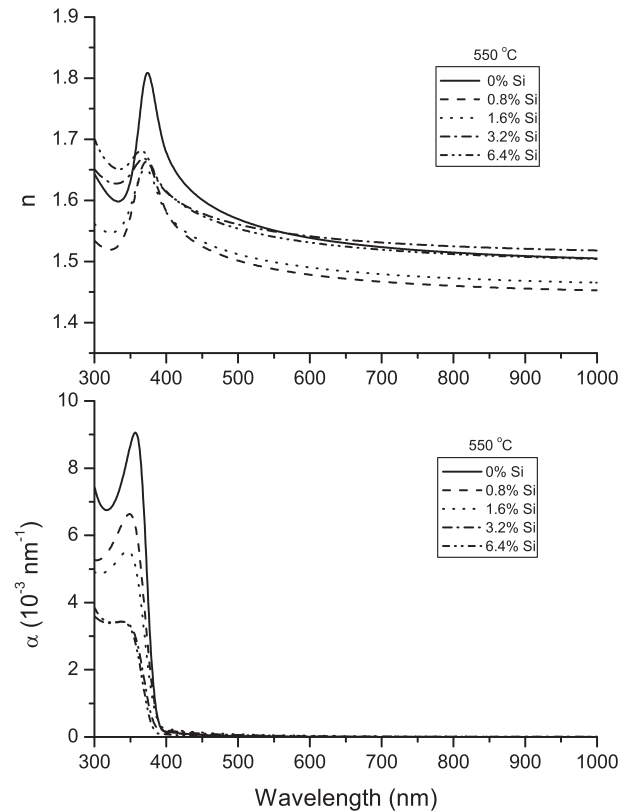

Fig. 7. Refractive index n and absorption coefficient α of ZnO:Si thin films annealed at 550 °C.

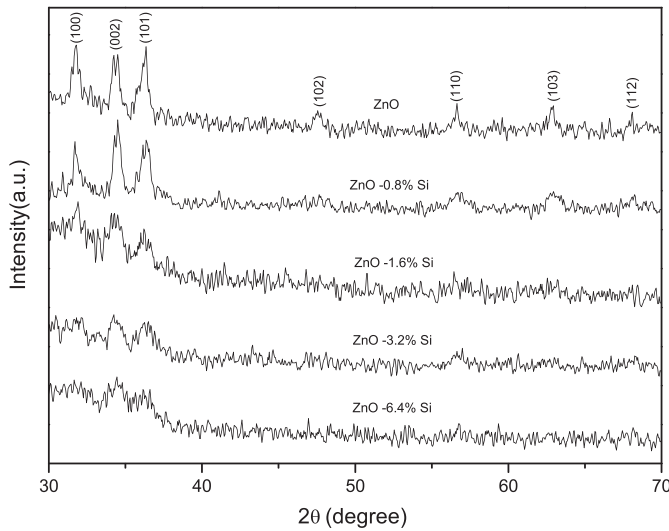

Fig. 8. XRD spectra of ZnO:Si thin films annealed at 550 °C.

gels. All coatings were prepared at room temperature (≈ 20 °C) and a relative humidity of 46%.

The transmittance and reflectance of the films were measured in the spectral range of 300–1000 nm using an NKD 7000 (Aquila, UK) spectrophotometer. The thickness, refractive index and absorption coefficient values of the films were determined by fitting to the DTLU model [16], as described in the next section. AFM images of the films were obtained using an SPM-9500J3 (Shimadzu, Japan) scanning probe microscope in contact mode. The structures of the films were analyzed by an X-ray diffractometer (GBC-MMA, CuKα radiation).

3. Theoretical model

The reflectance and transmittance data gathered by the spectrophotometer can be related to the optical characteristics of the film by fitting with an appropriate choice of the film dielectric function—in our case a variant of the Tauc–Lorentz (TL) oscillator model [19]. The imaginary part of the TL dielectric function is a product of Tauc law [20] and Lorentz oscillator terms, an approximation intended to capture the optical behavior both near and significantly above the band gap. The TL model has been successfully applied to a variety of semiconductors and optical coating materials [21,22], among them ZnO [23]. It was extended by Ferlauto *et. al.* to incorporate an exponential Urbach tail in the sub-gap region, the so-called Tauc–Lorentz–Urbach (TLU) model [17]. The TLU model has been shown to work quite well on pure sol–gel-derived ZnO thin films [3]. For the ZnO:Si system we found that accurate fitting to the experimental data could be accomplished through a DTLU dielectric function, consisting of a combination of one TL and one TLU oscillator. The technical details of the DTLU model are given in Ref. [16], where it was developed to analyze WO_3 coatings, so we only give a brief overview here.

The DTLU dielectric function $\epsilon(E)$, as a function of photon energy E, consists of real and imaginary parts: $\epsilon(E) = \epsilon_1(E) + i\epsilon_2(E)$. We only need to explicitly specify the imaginary part, $\epsilon_2(E)$, since $\epsilon_1(E)$ is related to $\epsilon_2(E)$ through the Kramers–Kronig integral:

$$\epsilon_1(E) = \epsilon_{1\infty} + \frac{2}{\pi} P \int_0^\infty d\xi \, \frac{\xi \epsilon_2(\xi)}{\xi^2 - E^2} . \tag{1}$$

P is the Cauchy principal value of the integral, and $\epsilon_{1\infty} = 1$ by physical constraint [17].

The explicit form of the imaginary part is given by a sum of TL and TLU contributions, $\epsilon_2(E) = \epsilon_{2TL}(E) + \epsilon_{2TLU}(E)$, where [19]:

$$\epsilon_{2TL}(E) = \begin{cases} \dfrac{A_1 E_{01} \Gamma_1 (E - E_{g1})^2}{E\left[\left(E^2 - E_{01}^2\right)^2 + \Gamma_1^2 E^2\right]} & \text{for } E > E_{g1}, \\ 0 & \text{for } E \le E_{g1}. \end{cases} \tag{2}$$

and [17]:

$$\epsilon_{2TLU}(E) = \begin{cases} \dfrac{A_2 E_{02} \Gamma_2 (E - E_{g2})^2}{E\left[\left(E^2 - E_{02}^2\right)^2 + \Gamma_2^2 E^2\right]} & \text{for } E > E_t, \\ \dfrac{E_c}{E} \exp\left(\dfrac{E - E_t}{E_u}\right) & \text{for } E \le E_t. \end{cases} \tag{3}$$

All the fitting parameters have dimensions of energy, and can be described as follows: both TL and TLU expressions are parametrized by the band gap E_{gi}, $i = 1, 2$, and the Lorentz oscillator amplitude A_i, resonance energy E_{0i}, and oscillator width Γ_i. The TLU term has an exponential Urbach tail at lower energies, with two additional fitting parameters: E_t is the cutoff above which the Urbach tail ends and interband transitions begin; E_u sets the width of the Urbach tail. The coefficient E_c is set by the constraint that $\epsilon_{2TLU}(E)$ is continuous at $E = E_t$.

For completeness, we included the possibility of significant surface roughness by dividing the film into two layers: a region of thickness d, described by the DTLU dielectric function $\epsilon(E)$, and an overlayer of thickness d_{rough} made of 50% material, 50% voids [24]. This overlayer has a dielectric function $\epsilon_{rough}(E)$ related to $\epsilon(E)$ through the Bruggeman effective medium approximation [25]:

$$\frac{1}{2}\left(\frac{1 - \epsilon_{rough}}{1 + 2\epsilon_{rough}}\right) + \frac{1}{2}\left(\frac{\epsilon - \epsilon_{rough}}{\epsilon + 2\epsilon_{rough}}\right) = 0. \tag{4}$$

The corrections to the theoretically predicted reflectance and transmittance due to the assumed surface roughness overlayer are sufficiently small that it is not always possible to extrapolate a reliable, non-zero value for d_{rough} from the experimental measurements. In fact, the only cases where the overlayer noticeably helped in the fitting were the Si-doped 550° C films. For all other samples a model without an overlayer was sufficient. If both layers are present, there are a total of twelve free parameters: A_1, E_{01}, E_{g1}, Γ_1, A_2, E_{02}, E_{g2}, Γ_2, E_t, E_u, d, d_{rough}.

In deriving reflectance and transmittance from the parameters of our theoretical dielectric function, we take into account intensity attenuation due to large near-UV absorption by the glass substrate, as described in Ref. [26]. The least-squares fitting of the model parameters to the experimental data is carried out through the Levenberg–Marquardt multivariate-regression algorithm. We can thus obtain best-fit results for the film refractive index n and absorption coefficient α over the measured spectral range, which are related to ϵ_1 and ϵ_2 through:

$$\begin{aligned} n &= \left[\frac{(\epsilon_1^2 + \epsilon_2^2)^{1/2} + \epsilon_1}{2}\right]^{1/2} \\ \alpha &= \frac{2E}{\hbar c}\left[\frac{(\epsilon_1^2 + \epsilon_2^2)^{1/2} - \epsilon_1}{2}\right]^{1/2} . \end{aligned} \tag{5}$$

Note that the bandgap parameters E_{g1} and E_{g2} which appear in the TL and TLU oscillators only roughly correspond to actual physical band gaps [17,21,27], since both these oscillators are approximate mathematical models. However, we can get a reasonable estimate of the bandgap by looking at $\alpha(E)$ as a function of photon energy E. Near the onset of large absorption (where the exponential tail ends) it behaves like $\alpha(E) \propto E^{-1}(E - E_g)^{1/2}$, the scaling form corresponding to the direct transition seen in ZnO and

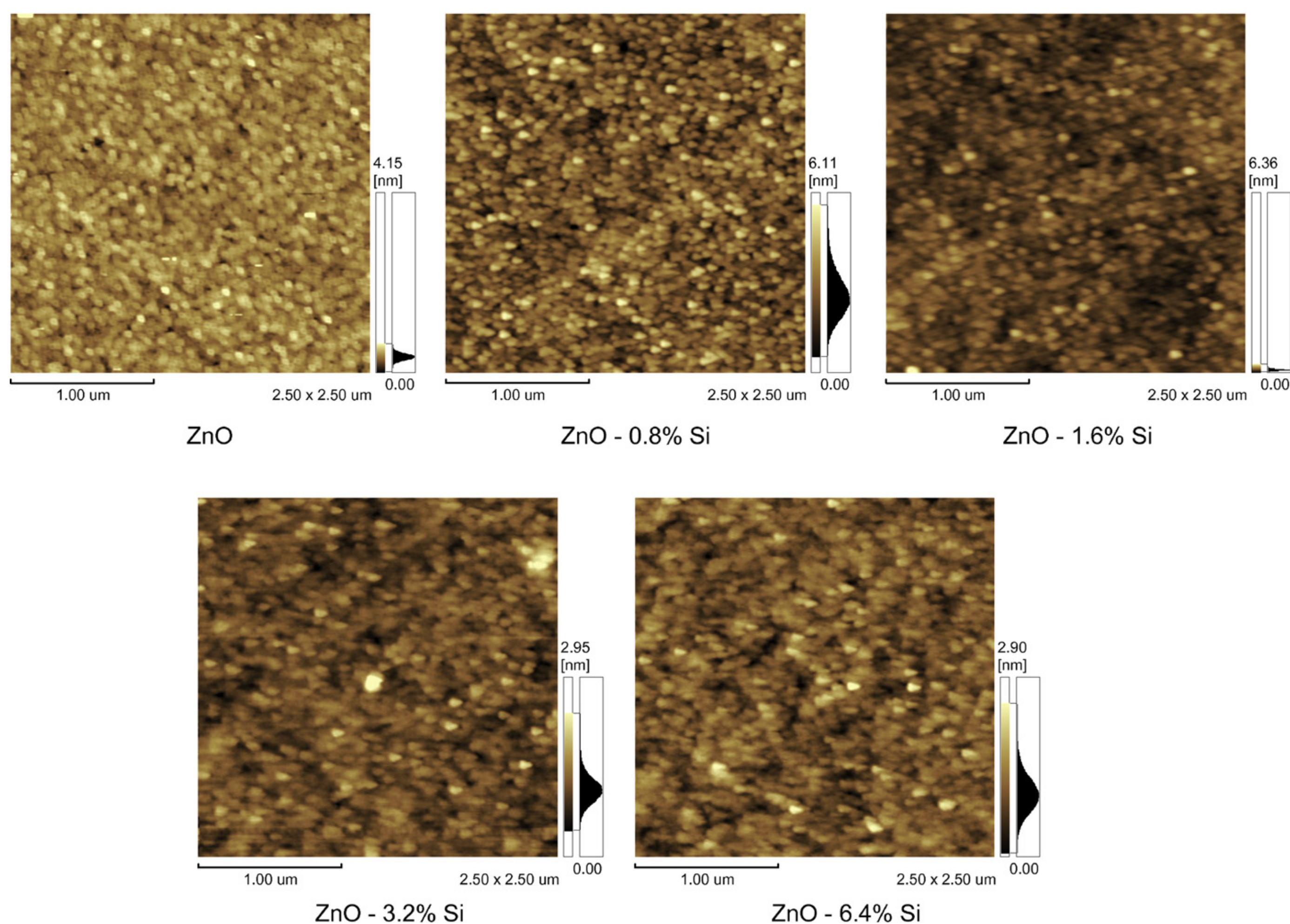

Fig. 9. AFM images of ZnO:Si thin films annealed at 350 °C.

ZnO:Si films. We can thus plot $(E\alpha(E))^2$ versus E, and perform a linear extrapolation to the intercept in order to find the value of E_g.

All the best-fit model parameters are listed in Tables 1–2, and Table 2 shows in addition the extrapolated bandgap E_g and values of n and α at particular wavelengths.

4. Results and discussion

4.1. Optical properties

The transmittance and reflectance spectra of ZnO:Si films heat treated at 250 ° C can be seen in Fig. 2. Though the spectra vary slightly with the level of doping, there is no obvious trend. The transmittance is between 85 and 87% and the reflectance is around 10–12% in the visible region. The spectra in Figs. 3 and 4 belong to films heat treated at 350 and 550 °C, respectively. Unlike the 250 ° C results, a clear contrast is evident between the pure and doped samples, with the presence of Si leading to higher transmittance and lower reflectance across the entire wavelength range relative to the pure ZnO film. The pattern is particularly evident in the 550 ° C curves of Fig. 4, where the transmittance increases monotonically from 83.6% to 90% at $\lambda = 400$ nm and 87.5% to 90% at $\lambda = 550$ nm as the doping varies from 0% to 6.4% Si.

The increased transmittance at higher annealing temperatures might be due to changes in the crystal structure arising from doping. The Si^{4+} ions have a significantly smaller ionic radius ($r_{Si^{4+}} = 0.04$ nm) compared to the Zn^{2+} ions ($r_{Zn^{2+}} = 0.074$ nm) [28]. As a result Si doping causes stress in the ZnO lattice, degrading its crystal structure (as will be seen below in the XRD results) and leading to segregation of the dopant toward particle boundaries [29]. The sharp dip in both transmittance and reflectance below $\lambda \approx 380$ nm in the pure films, associated with the excitonic absorption of ZnO [30], is much less pronounced in the doped samples—a consequence of the decreased crystallinity. This weaker excitonic absorption is most evident in the dramatic increases in transmittance (as much as 20–50% larger than pure ZnO) in the near-UV region for the 350 and 550 ° C films. The 250 ° C film, which is inherently more disordered regardless of doping, does not show a steep exciton-related dip, nor a clear transmittance difference as dopant concentration is increased.

Refractive indices n and absorption coefficients α of the ZnO:Si thin films are plotted in Figs. 5–7 for the three different annealing temperatures. Particular values of n (at 550 nm), α (at 350 nm), and the band gap E_g are listed in Table 2. We see the same distinction between the 250 ° C results and the ones at higher temperatures. Pure ZnO heat treated at 250 ° C has relatively small near-UV absorption, $\alpha \lesssim 0.6 \times 10^{-3}$ nm^{-1} for $\lambda = 300-400$ nm, and a refractive index with normal dispersion over the entire range, decreasing from 1.66 to 1.55 from $\lambda = 300$ to 1000 nm. Qualitatively, the doped films are similar, except that near-UV absorption

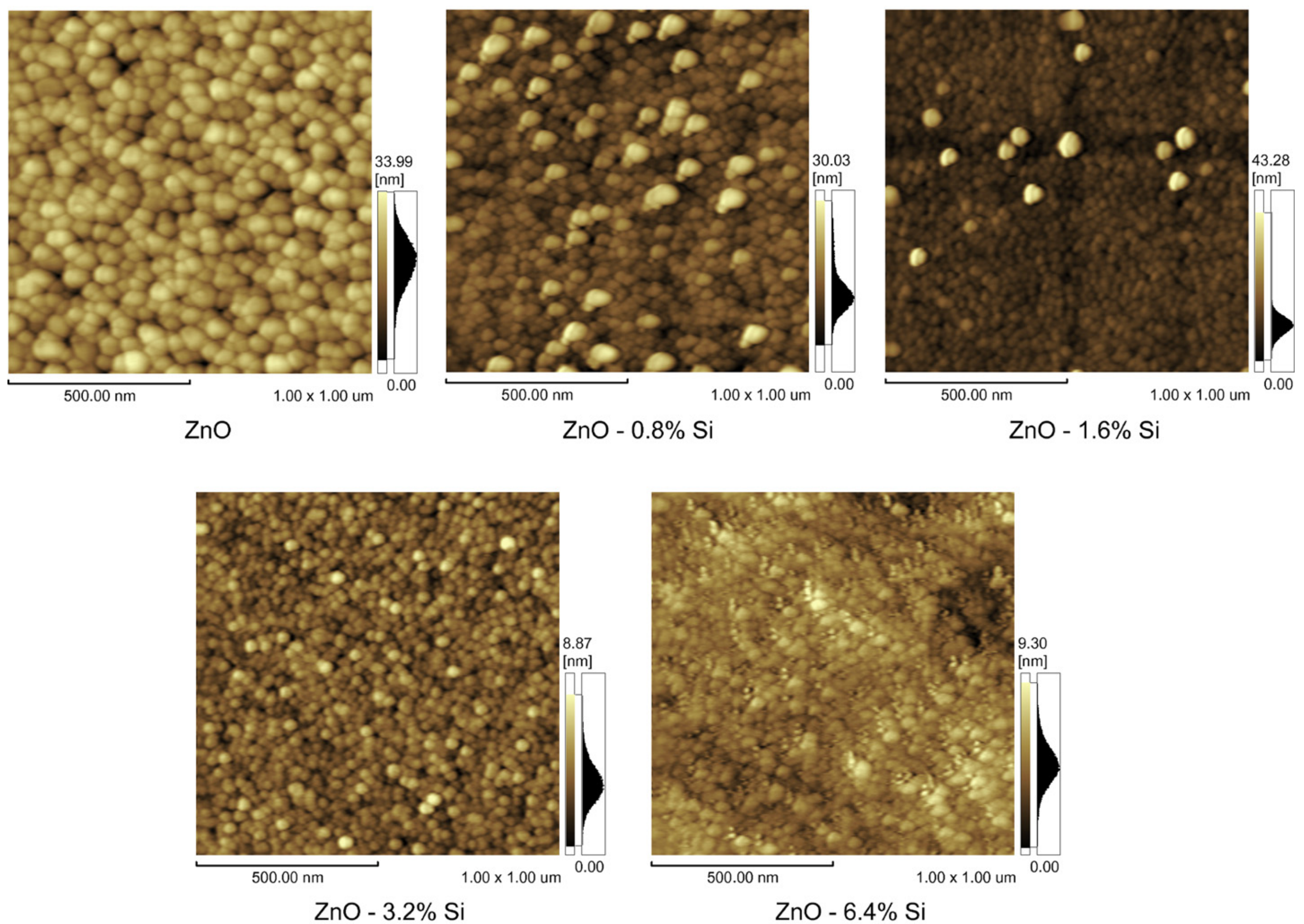

Fig. 10. AFM images of ZnO:Si thin films annealed at 550 °C.

increases with doping (roughly doubling at 6.4% Si) and n is pushed up by 0.03–0.08.

For the 350 and 550° C films, on the other hand, excitonic absorption leads to markedly higher α, between $\approx$ 4 and 9 $\times 10^{-3}$ nm^{-1} for $\lambda \lesssim 380$ nm. Instead of increasing with doping, the absorption actually decreases (the weakening of the excitonic effect discussed above). Going from 0% to 6.4% Si doping at $\lambda = 350$ nm, α drops about 40% for the 350° C case, and 60% for the 550° C case. The refractive index exhibits anomalous dispersion in the near-UV region, associated with the steep onset of absorption. In the visible region, the n values are comparable for all three annealing temperatures and doping levels, i.e. at $\lambda = 550°$ nm they range between 1.49 and 1.62. These are compatible with earlier results for pure ZnO films, for example n(550nm) = 1.53 for a sol–gel coating at annealing temperature 550° C [31]. At 350 and 550° C the refractive index upon doping is generally smaller than the pure films (though the pattern is violated by the 3.2% and 6.4% Si-doped samples at 550° C for larger wavelengths).

The band gap for the pure ZnO film heat treated at 550° C is 3.29 eV, which agrees with the values found for sol–gel coated ZnO films annealed at the same temperature [32–34]. For 350° C the band gap is nearly identical, 3.31 eV, but falls to 3.15 eV at 250 °C, where the absorption edge is much shallower. Doping increases the band gap at all three temperatures, with the biggest change at 250° C (a shift up of 0.17 eV), and more modest shifts of 0.05 eV for the other cases. Note that the fitting to the experimental data always yields a small ($\lesssim 0.1 \times 10^{-3}$ nm^{-1}) exponential absorption tail in the sub-gap region—hence the necessity of using the DTLU model with its Urbach tail contribution, rather than just two TL oscillators.

4.2. Structural properties

Previous studies have shown that ZnO films crystallize at 400 ° C [18,35]. Consistent with this, our XRD measurements revealed that all the pure and Si-doped ZnO films heat treated at 250° C and 350° C are amorphous. In contrast, the XRD spectra of the 550° C films, plotted in Fig. 8, show clear signatures of crystallinity (pronounced peaks) at lower dopings. For higher dopings (1.6–6.4% Si), the crystal structure deteriorates. The intensity of the peaks at 31.8°, 34.4°, and 36.3° decreases significantly; the peaks at 47.5°, 56.6°, 62.9° and 68° almost vanish. The ZnO crystal planes corresponding to these seven angles are (1 0 0), (0 0 2), (1 0 1), (1 0 2), (1 1 0), (1 0 3), and (1 1 2), respectively, agreeing with earlier measurements on pure ZnO [18,36]. Even at the highest doping (6.4% Si), there were no crystal planes observed belonging to SiO_2. The decrease in crystallinity at higher dopings mirrors the sharp reduction of near-UV absorption mentioned earlier, supporting the structural interpretation of the observed optical trends (at least at 550 °C, and perhaps at 350 °C, where the overall structure is amorphous, but sufficient local ordering exists to see a sharp excitonic absorption edge.)

AFM measurements on the ZnO:Si films, shown in Fig. 9 (350 °C) and Fig. 10 (550 °C), reveal a small variation in surface conditions. (The corresponding RMS roughness values are listed in Table 2.) All the samples heat treated at 350° C and below are relatively

smooth (RMS $\lesssim$1 nm), with the exception of pure ZnO at 250 °C, where the RMS is 7 nm. The 550 ° C films are relatively rough at smaller dopings (RMS ≈5 nm), but become smoother at 3.2% and 6.4% Si.

Doping at any given temperature does not have a clear impact on the thickness of the films (Table 2), though films annealed at 250 ° C are ≈2 – 3 times thicker than those treated at higher temperatures—as expected from the TGA results of Fig. 1, which show that significant evaporation of residual material sets in above 250 °C.

5. Conclusions

Si-doped ZnO films were produced using the sol–gel spin coating method. The optical and structural properties of these transparent thin films were characterized at various annealing temperatures – 250, 350, and 550 ° C – and Si doping levels up to 6.4%. An extension of the Tauc–Lorentz dielectric function, including two oscillator terms and a sub-gap absorption tail, was found to accurately fit experimental reflectance and transmittance data across the entire parameter range. There were clear qualitative differences between the 250 ° C films and those at higher temperatures. The former exhibited an increased refractive index and near-UV absorption upon doping, while in the latter cases this trend was generally reversed. The 550 ° C films showed a progressive increase in transmittance and decrease in reflectance with doping, both in the near-UV and visible regions. Significant transmittance gains in the near-UV range (20–50% larger than pure ZnO) were associated with a decrease in excitonic absorption. This decrease is linked to dopant-induced changes in the crystal structure, revealed by XRD: the 550 ° C films were ordered at low dopings, but the crystallinity steadily degraded from 1.8% to 6.4% Si. For annealing temperatures lower than 550 °C, the films were amorphous. At all temperatures, the band gaps were shifted up with doping, though for 350 and 550 ° C the values remained within 2% of 3.3 eV, the band gap for pure ZnO. AFM measurements indicated that the doped 550 ° C films had rougher surfaces at than their counterparts at 250 ° C and 350 °C.

Acknowledgements

Istanbul Technical University generously supported this research. We also thank Prof. Dr. Sabriye Pişkin for allowing us to use the TGA system.

References

[1] J.M. Lee, B.H. Choi, M.J. Ji, J.H. Park, J.H. Kwon, B.K. Ju, Semicond. Sci. Technol. 24 (2009) 055008, 1–5.
[2] X. Ju, W. Feng, X. Zhang, V. Kittichungchit, T. Hori, H. Moritou, A. Fujii, M. Ozaki, Sol. Energy Mater. Sol. Cells 93 (2009) 1562–1567.
[3] D. Saygin-Hinczewski, M. Hinczewski, I. Sorar, F.Z. Tepehan, G.G. Tepehan, J. Optelectron. Adv. Mater. Symp. 1 (2009) 382–385.
[4] T. Minami, H. Sato, H. Nanto, S. Takata, Jpn. J. Appl. Phys. 25 (1986) L776–L779.
[5] H. Sato, T. Minami, S. Takata, J. Vac. Sci. Technol. 11 (1993) 2975–2979.
[6] A.K. Das, P. Misra, L.M. Kukreja, J, Phys. D: Appl. Phys. 42 (2009) 1–7.
[7] J. Nomoto, T. Miyata, T. Minami, J. Vac. Sci. Technol. A 27 (2009) 1001–1005.
[8] M. Abdullah, S. Shibamoto, K. Okuyama, Opt. Mater. 26 (2004) 95–100.
[9] C. Cannas, M. Mainas, A. Musinu, G. Piccaluga, Compos. Sci. Technol. 63 (2003) 1187–1191.
[10] T. Tani, L. Madler, S.E. Pratsinis, J. Mater. Sci. 37 (2002) 4627–4632.
[11] J. Zhao, L. Qin, L. Zhang, Physica E 40 (2008) 795–799.
[12] C. Brinker, G. Scherer, Sol–Gel Science: The Physics and Chemistry of Sol–Gel Processing, Academic Press, San Diego, 1990.
[13] Y.S. Kim, W.P. Tai, S.J. Shu, Thin Solid Films 491 (2005) 153–160.
[14] J.H. Lee, K.H. Ko, B.O. Park, J. Cryst. Growth 247 (2003) 119–125.
[15] S.W. Xue, X.T. Zu, W.L. Zhou, H.X. Deng, X. Xiang, L. Zhang, H. Deng, J. Alloys Compd. 448 (2008) 21–26.
[16] D. Saygin-Hinczewski, M. Hinczewski, I. Sorar, F.Z. Tepehan, G.G. Tepehan, Sol. Energy Mater. Sol. Cells 92 (2008) 821–829.
[17] A.S. Ferlauto, G.M. Ferreira, J.M. Pearce, C.R. Wronski, R.W. Collins, X. Deng, G. Ganguly, J. Appl. Phys. 92 (2002) 2424–2436.
[18] I. Sorar, F.Z. Tepehan, Optelectron. Adv. Mater. Rapid Commun. 3 (2009) 455–458.
[19] G.E. Jellison, F.A. Modine Jr., Appl. Phys. Lett. 69 (1996) 371–373.
[20] J. Tauc, Optical Properties of Solids, Elsevier, Amsterdam, 1970.
[21] H. Chen, W.Z. Shen, Eur. Phys. J. B 43 (2005) 503–507.
[22] B. von Blanckenhagen, D. Tonova, J. Ullmann, Appl. Opt. 41 (2002) 3137–3141.
[23] J.P. Zhang, G. He, L.Q. Zhu, M. Liu, S.S. Pan, L.D. Zhang, Appl. Surf. Sci. 253 (2007) 9414–9421.
[24] G.E. Jellison, V.I. Merkulov, A.A. Puretzky, D.B. Geohegan, G. Eres, D.H. Lowndes, J.B. Caughman Jr., Thin Solid Films 377–378 (2000) 68–73.
[25] D.A.G. Bruggeman, Ann. Phys. (Leipzig) 24 (1935) 636–679.
[26] D.S. Hinczewski, M. Hinczewski, F.Z. Tepehan, G.G. Tepehan, Sol. Energy Mater. Sol. Cells 87 (2005) 181–196.
[27] Z.G. Hu, J.H. Ma, Z.M. Huang, Y.N. Wu, G.S. Wang, J.H. Chu, Appl. Phys. Lett. 83 (2003) 3686–3688.
[28] R.D. Shannon, Acta Crystallogr. A 32 (1976) 751–767.
[29] J.H. Lee, B.O. Park, Thin Solid Films 426 (2003) 94–99.
[30] S.-Y. Kuo, W.-C. Chen, C.-P. Cheng, Superlattices Microstruct. 39 (2006) 162–170.
[31] S. Bandyopadhyay, G.K. Paul, S.K. Sen, Sol. Energy Mater. Sol. Cells 71 (2002) 103–113.
[32] G.K. Paul, S.K. Sen, Mater. Lett. 57 (2002) 959–963.
[33] G.K. Paul, S. Bandyopadhyay, S.K. Sen, S. Sen, Mater. Chem. Phys. 79 (2003) 71–75.
[34] A.Y. Oral, Z.B. Bahşi, M.H. Aslan, Appl. Surf. Sci. 253 (2007) 4593–4598.
[35] D. Raoufi, T. Raoufi, Appl. Surf. Sci. 225 (2009) 5812–5817.
[36] M. Dutta, T. Ghosh, D. Basak, J. Electron. Mater. 38 (2009) 2335–2342.